

## Global Properties of High Liquid Loading Turbulent Crude Oil + Methane/Air Spray Flames

P. DUTTA, J. P. GORE\*, Y. R. SIVATHANU, and P. E. SOJKA

*Thermal Sciences and Propulsion Center, School of Mechanical Engineering, Purdue University, West Lafayette, IN 47907*

Measurements of atomization quality, flame heights, radiative fractions, emission temperatures, and transmittance for Alberta sweet crude oil/methane flames established on a novel burner for simulating well-blowout fires are reported. The results show the effects of two-phase flow on flame heights. The measurements of radiative fractions and the optical properties suggest relatively low soot loading. The measured high temperatures suggest almost complete combustion of crude-oil. However, larger-scale tests as well as information concerning the physical processes in the present atomizer and burner are essential for the application to practical fires and combustion devices.

### NOMENCLATURE

$d$	external orifice diameter
$g$	acceleration due to gravity
Fr	Froude number, $Fr = u^2/gd$
$H_f$	visible flame height
HLR	hydrogen-to-liquid ratio by mass
MLR	methane-to-liquid ratio by mass
$N$	Rosin-Rammler drop-size distribution parameter
$Q_f$	heat release rate
SMD	Sauter mean diameter
$u$	nozzle exit velocity
$x$	distance from the nozzle exit
$X$	characteristic diameter in Rosin-Rammler distribution
$X_R$	fraction of chemical energy lost to the surrounding by radiation.

### INTRODUCTION

Oil-well blowout fires during drilling, production or workover present a serious hazard to personnel, environment, and equipment, particularly on off-shore platforms [1, 2]. Typical oil-well blowout fires involve combustion of a mixture of liquid and gaseous fuels. The atomization of the liquid is caused by the expansion of the mixture to atmospheric pressure. Heat transfer from the combustion zone established

by the gaseous components and the fuel vapor in conjunction with the atmospheric oxygen causes evaporation of the atomized liquid fuel. The infrared radiation energy leaving the resulting fires is hazardous to the platform, equipment and personnel.

Typically, material exiting an oil-well consists of 80% to 95% liquid with 20% to 5% gases and vapors by mass. In the absence of wind, the material expands in a vertical jet configuration, mixes with the surrounding air, and forms turbulent jet diffusion flames stabilized at or above the well head. As previously observed in blowout fires and more recently in the oil-well fires in Kuwait, the liquid atomizes and evaporates effectively in this configuration and flames are stabilized. These jets represent high-liquid-loading dense sprays that have not been studied in the literature extensively [3].

The flame height, size, and radiation properties of high-liquid-loading two-phase flames have not received much attention in the literature except for the study of Hustad and Sonju [4], involving global property measurements for relatively large-scale (1–8 MW) oil/gas flames. In that study, the oil and the gas were mixed in a chamber upstream of a large-diameter (10–33 mm) nozzle exit. In such a configuration, the quality of atomization changes with liquid loading and exit diameter. The measurements of visible flame heights by Hustad and Sonju [4] showed that the two-phase flames are much longer than gaseous flames with similar heat

\* Corresponding author.

release rates. However, due to the large size of the flames, information concerning drop sizes and the extent to which the distance needed for evaporation of the fuel affected the flame heights could not be obtained.

Laboratory tests of two-phase spray flames have been restricted to relatively low-liquid-loading since conventional twin-fluid atomizers require high kinetic energy of the gas phase for effective atomization. Therefore, liquid mass fraction in the incoming stream has been restricted to 0.5 in past intermediate-scale and laboratory-scale tests [2, 5]. Attempts to increase the liquid loading resulted in large drops. A large amount of unburned crude-oil also exited the flame due to lack of efficient evaporation. Therefore, an effervescent atomizer-burner was developed in the present study for the establishment of high-liquid-loading crude-oil jet flames in the laboratory.

In oil reservoirs, dissolved gases and light components exist in the form of small bubbles, which are similar to those found in effervescent atomizers. The high-pressure oil-gas mixture exits from a long passage into an atmospheric pressure environment in oil-well fires, which is simulated by the effervescent atomizer-burner. Matching the conditions between the two any further would require detailed measurements of actual oil-well fires that are unavailable.

The effervescent atomizer concept and design followed the work of Lund et al. [6]. As discussed above, a study of the flames stabilized on this burner is expected to improve the understanding of oil-well blowout fires due to the inherent similarity in the atomization and combustion processes.

A second limitation on the similarity between the laboratory and the practical oil-well flames is introduced by consideration of flame liftoff and blowout. Although liftoff and blowout characteristics of two-phase jet fires have not been studied, based on the work of McCaffrey and Evans [7] for gaseous jet flames, it can be conjectured that the effects of burner size will be significant. McCaffrey and Evans [7] have shown that for natural gas-air flames, liftoff and blowout are observed with increasing exit velocity for tube diameters below 38 mm. This limit implies that all laboratory flames

except those burning hydrogen or acetylene liftoff at velocities lower than those of practical interest in many applications. Laboratory studies of attached gaseous diffusion flames have therefore relied on pilot flames, both non-premixed [8] and premixed [9], to overcome the liftoff and blowout problems. Similarly, the present two-phase laboratory jet fires must rely on a pilot flame that the practical oil-well blowout fires do not require.

The objectives of the present article are (1) to describe a successful design of the atomizer-burner, (2) to discuss global properties (visible flame height, radiative fractions) of the crude-oil/methane flames stabilized on the burner, and (3) to report path-integrated measurements of emission temperature and monochromatic transmittance to help understand the behavior of the radiative fractions. The present results for the visible flame height are also compared with the correlations of Hustad and Sonju [4] to highlight the effects of the atomization quality on the flame length.

## EXPERIMENTAL METHODS

A sketch of the effervescent atomizer-burner is shown in Fig. 1. The effervescent atomization portion of the burner follows the design of

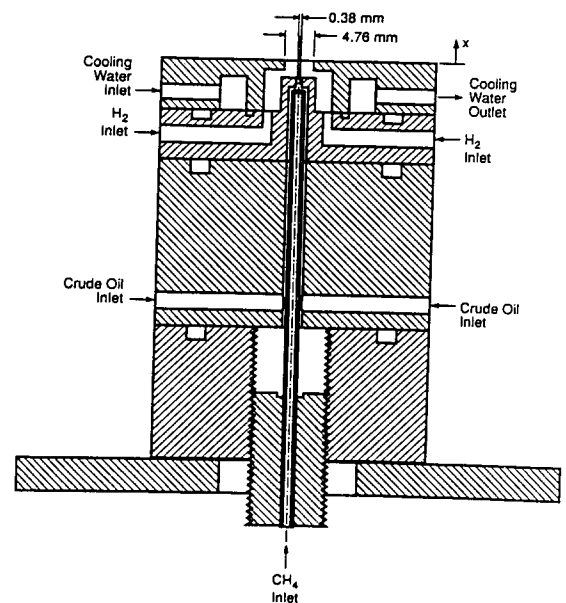


Fig. 1. Sketch of the effervescent atomizer-burner.

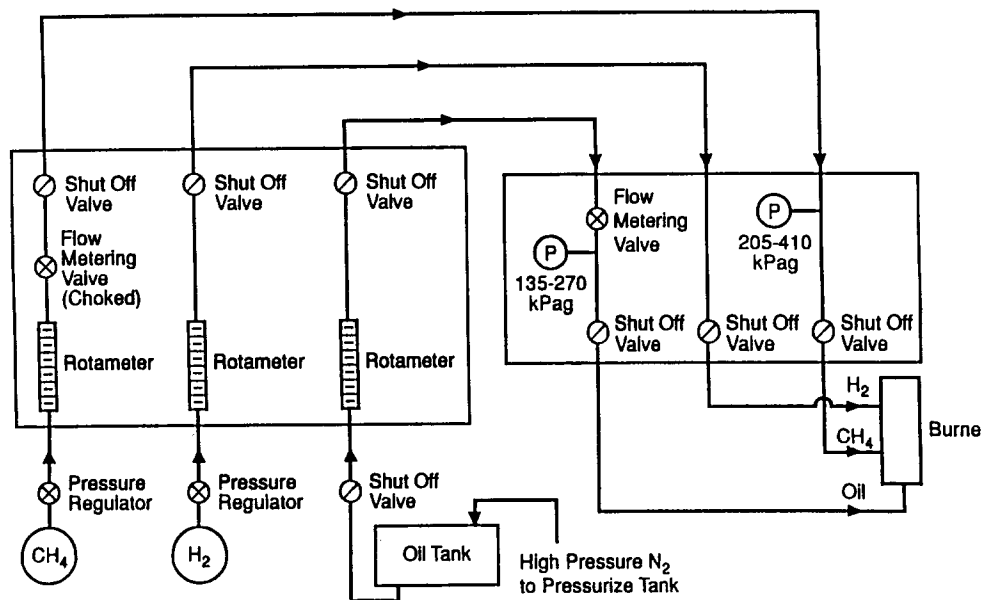
Lund et al. [6] closely. The crude oil flows into an annular space formed by the body of the burner and the central methane injection tube. The methane injection tube is similar to the aeration tube of Lund et al. [6]. Aeration is achieved by drilling multiple holes on the methane injector tube.

Small pool fires were observed around the oil-well fires in Kuwait. The crude-oil jet flames were stabilized by these small pool fires. In order to stabilize the flame on the burner port, a small ring flame of hydrogen is utilized. Use of a pool flame instead of a hydrogen ring would simulate an oil-well fire even more closely. The two-phase crude-oil-methane flow exits the central 0.38-mm orifice and flows through the ring flame resulting in a jet flame attached to the 4.76-mm diameter exit port of the burner. The top plate of the burner is cooled by a small flow of water flowing through an annular space to avoid fuel coking near the orifice.

Figure 2 is a schematic of the flow system used to control the pressures and the mass flow rates of crude oil, methane, and hydrogen flowing into the burner. The crude oil is stored

in a tank rated for 2 MPa. The liquid in the tank is pressurized using nitrogen connected to the gas space of the tank via a pressure regulator. The pressure in the tank is thus maintained by admitting nitrogen into the tank as the liquid is used. The liquid flow-rate is metered by a Nupro "S" series Fine Metering Valve. A shutoff valve is included so that the metering position can be maintained from one test to another. The flow-rate is monitored by a calibrated rotameter. The liquid pressure just upstream of the burner was monitored to be between 135 and 270 kPag using an inline pressure gauge for all the tests reported here. The methane gas pressure upstream of the burner was between 205 and 410 kPag and the hydrogen pressure was approximately 138 kPag. The mass flow rate of methane is governed by a choked metering valve mounted downstream of a rotameter. The hydrogen flow is also monitored by a rotameter.

Table 1 shows the operating conditions for the flames studied during the present investigation. The mass flow rate of the atomizing methane varied between 5% and 20% of the mass flow rate of the crude-oil. The Alberta



Schematic of Flow System

Fig. 2. Schematic of the flow control system for the effervescent atomizer burner.

TABLE I  
Operating Conditions

Test Case	$\dot{m}_{\text{oil}}$ (mg/s)	$\dot{m}_{\text{CH}_4}$ (mg/s)	MLR (%)	$\text{Re}_d^a$ $d = 4.76 \text{ mm}$	$\text{Re}_d$ $d = 0.38 \text{ mm}$	$Q_f$ (kW)	$X_R$ (%)
1	135	27.0	20	$3.8 \times 10^3$	$1.8 \times 10^4$	9.2	11.4
2	234	32.8	14	$5.5 \times 10^3$	$2.3 \times 10^4$	14.2	10.2
3	238	23.8	10	$4.9 \times 10^3$	$1.8 \times 10^4$	13.5	15.5
4	250	25.0	10	$5.1 \times 10^3$	$1.9 \times 10^4$	14.0	14.0
5	260	13.0	5	$4.8 \times 10^3$	$1.1 \times 10^4$	13.9	21.4
6	328	16.4	5	$5.4 \times 10^3$	$1.3 \times 10^4$	17.0	20.7
7	360	18.0	5	$5.7 \times 10^3$	$1.5 \times 10^4$	18.5	20.6
8 <sup>b</sup>	400	20.0	5	$6.9 \times 10^3$	$1.6 \times 10^4$	21.0	19.5

$$^a \text{Re}_d = \frac{\rho_{\text{TP}} V_{\text{TP}} d}{\mu_{\text{TP}}}$$

<sup>b</sup> Higher hydrogen flow-rate.

sweet crude oil has a density of 840 kg/m<sup>3</sup>, viscosity of 5 cP, and surface tension of 30 dyn/cm [10]. The hydrogen flow used for flame attachment did not affect the atomization quality significantly and was maintained at 16.4 mg/s for all the flames except the last. In order to stabilize the flame with the highest crude-oil flow, a higher flow of hydrogen (21.2 mg/s) was required. The heat release rates for the flames varied between 9 and 21 kW based on nominal heating values of 43,400 kJ/kg for the crude oil, 50,000 kJ/kg for methane, and 120,900 kJ/kg for hydrogen. The Reynolds number characteristic of the jet were evaluated based on the external orifice diameter (4.76 mm) on which the flame is stabilized or based on the diameter through which the two-phase material exits (0.38 mm). The Reynolds numbers based on both these diameters are listed in Table 1. The use of the larger diameter assumes that the material expands to fill the exit port while the use of the smaller diameter assumes that the jet is formed independent of the external orifice. The two different assumptions lead to Reynolds numbers differing by an order of magnitude. The issue of the appropriate characteristic dimension is not currently resolved, as discussed later.

The radiative heat flux distribution from the flames to the surface of a long imaginary cylindrical enclosure with a base aligned at the level of the burner (semiinfinite cylindrical enclosure) was measured using a Medtherm wide angle (150°) radiometer. The resulting data were integrated to obtain the total energy radi-

ated by the flames. The details of the measurement technique and the geometry of traverse of the radiometer have been discussed in detail by Sivathanu and Gore [11]. The uncertainties in these measurements are less than 10% based on the least count of the data acquisition system. The radiative fractions ( $X_R$ ) obtained from these measurements are listed in Table 1. These vary from approximately 10% for the flames with the highest methane loading to approximately 20% for the flames with the highest crude-oil loading. These values are relatively low, indicative of highly forced jets. However, measurements of velocities are needed to clarify further the issue of momentum versus buoyancy effects.

The atomizer-burner was operated in a cold-spray configuration facing downward (injecting in the direction of gravity) to evaluate its performance in terms of drop-size distributions. A Malvern 2600 particle size analyzer with a focal length 300 mm was used for these tests similar to previous work [6, 10]. The particle sizes were measured at a distance of 25 diameters (12 cm) downstream of the atomizer to ensure that most of the particles are spherical drops. Effects of total oil flow rate and methane-to-oil mass-flow-rate ratio (MLR) on drop size distribution were studied.

The flames were stabilized with the burner facing vertically up (opposing the direction of gravity) in a screened enclosure of 1 m × 1 m × 2 m size with exhaust gas removal at the top. Past tests by Lund [12] have shown that the orientation does not affect the atomization

quality. The vertically up orientation is clearly preferred for the removal of the exhaust products as well as for simulating the actual oil-well fires. Flame heights were measured by first recording the flames using a charge coupled device (CCD) array video camera with the shutter speed set at 1000 Hz. Heights were then measured from the video screen and averaged over 40 frames with a measurement taken every five frames. The frames were 1/60th of a second apart. The video screen was appropriately scaled to provide actual flame heights. Uncertainties of the flame height measurements were found to be less than 7% based on the repeatability of the ensemble averages.

In order to examine the emission of smoke into the exhaust stream as well as understand the radiative fractions of different flames, measurements of path-integrated transmittance and path-integrated emission temperatures were obtained for diametric paths at various heights above the burner exit. The instrumentation used for these tests was developed by Sivathanu et al. [13]. However, instead of inserting the purged stainless-steel probes into the flame, the entire flame was observed to obtain path-integrated absorption and emission data.

A helium-neon laser (632.8 nm wavelength) with a chopper was used to obtain the monochromatic transmittance of the flames. The transmittance of the flames is lower than unity due to absorption by soot particles and intermediate hydrocarbon species, as well as scattering and absorption by the liquid oil drops along the path. In the parts of the flame that contribute to significant flame radiation, the reduction in the transmittance is dominated by absorption due to soot particles. Emission at 900 and 1000 nm is measured by two calibrated photomultiplier tubes with optical filters (100 nm band-width at half-peak transmittance). The emission data are used to infer the global temperature assuming specific absorption coefficients of soot particles given by Dalzell and Sarofim [14] and incorporating the transmittance curve of the filters into the calculation. These values have been found satisfactory for obtaining emission temperature data [15]. Possible interference from emission by hydrocarbon species other than soot particles was

neglected as a first step. Experimental uncertainties inherent to the three-wavelength instrument are discussed in Ref. [13].

## RESULTS AND DISCUSSION

Figure 3 shows the distribution of drop sizes measured by the Malvern analyzer at an axial location of  $x/d = 25$  along the centerline of the spray for three different liquid flow rates with a fixed methane-to-liquid flow rate ratio (MLR). The measurement of  $x$  is obtained from the base of the burner on which the flame is stabilized, to the location in the flame where the Malvern beam or other instruments

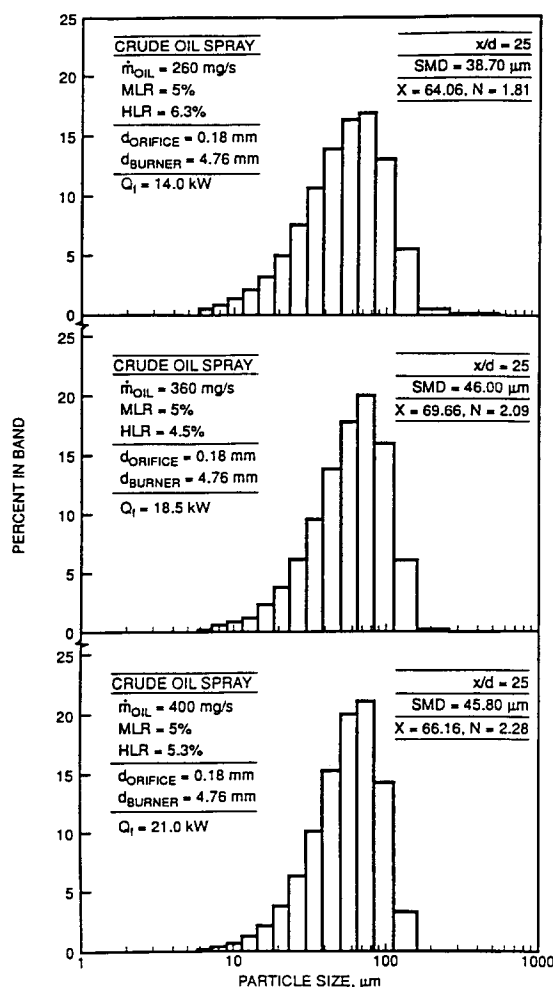


Fig. 3. Malvern measurements of drop size distributions for crude-oil sprays for three liquid flow rates with fixed methane-to-liquid ratio.

were positioned. The accuracy of the linear traverse used for measuring  $x$  is 1 mm. The measurements were made two times at every location and the typical change in the SMD was 3%–4%, which is within the range of accuracy of the Malvern particle sizer. Each measurement consisted of 1000 sweeps over a period of 8 s. The data were fit to a Rosin–Rammler drop-size distribution [16]. The Rosin–Rammler distribution may be expressed in the form

$$1 - Q = \exp - (D/X)^N,$$

where  $Q$  is the fraction of the total volume contained in drops of diameter less than  $D$ , and  $X$  and  $N$  are constants. The exponent  $N$  is a measure of the spread of drop sizes in the spray. The Rosin–Rammler parameters  $X$  and  $N$  are indicated on Fig. 3 for each drop-size distribution. The variation in  $X$  was between 2% and 8%, while the variation in  $N$  was between 2% and 12%. The effect of the changes in hydrogen flow rate were determined to be small (2  $\mu\text{m}$  change in SMD over the flow rate range 0 to operating condition) by turning this flow rate off during the drop size measurements. This is within the range of accuracy of the Malvern instrument. The Sauter mean diameter (SMD), which is significant in determining the evaporation rates, increases with the liquid flow rate between 260 and 360 mg/s but appears to stay almost constant between 360 and 400 mg/s. The resulting changes in evaporation length for the liquid drops may translate into differences in the visible flame heights, as will be seen later.

It was observed previously [10] that the ratio of methane-to-oil mass-flow rates affects the drop size more significantly than the total liquid flow rate. Figure 4 shows the drop size distribution measured by the Malvern analyzer for a fixed heat release rate of the flame ( $Q_f = 14 \text{ kW}$ ) and varying methane-to-oil mass ratios. For a MLR of 5%, the drops have an SMD of 38.70  $\mu\text{m}$ . This decreases to 26.90  $\mu\text{m}$  as the methane flow rate is increased to 10% and then to 23.70  $\mu\text{m}$  as the methane flow rate is increased further to 14%. It is therefore expected that the flame height will increase with decreasing methane-to-oil ratio (MLR).

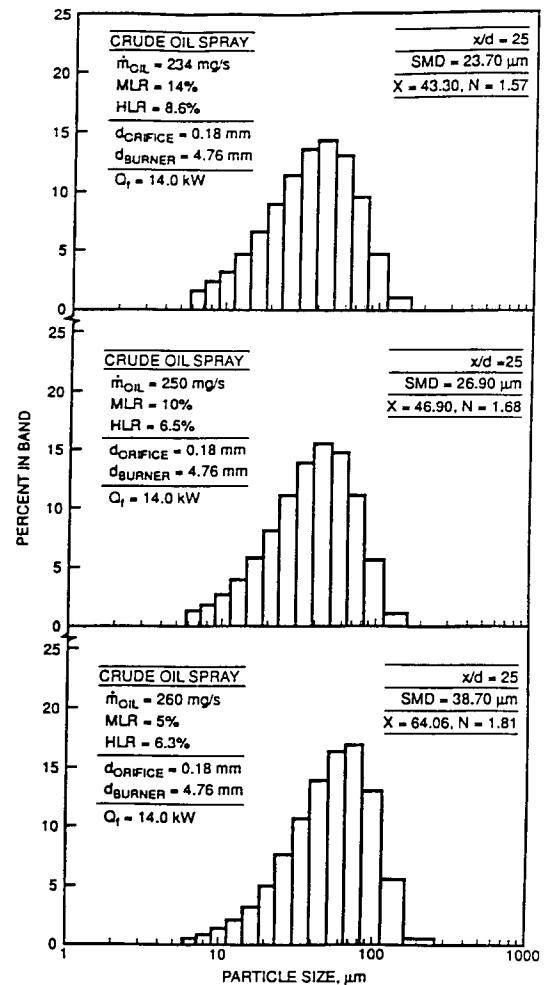


Fig. 4. Malvern measurements of drop size distributions for crude-oil sprays for three methane-to-liquid ratios with fixed heat release rate.

Figure 5 shows the flame height  $H_f$  normalized by the external orifice diameter  $d$  (4.76 mm) plotted as a function of the total heat release rate for the first seven flames in Table 1. The last flame had a higher flow of hydrogen for stabilization and hence is not considered together with the others. As seen in Fig. 5, the flames are taller for lower methane loading. For the methane loading of 5%, the flame height increases with heat release rates. This is probably due to the longer evaporation length needed because of the (1) higher mass-flow rate of oil and (2) larger drop size produced at higher liquid-flow rates. The height of buoyant jet flames burning gaseous fuels also increases with heat release rate due to the slower rela-

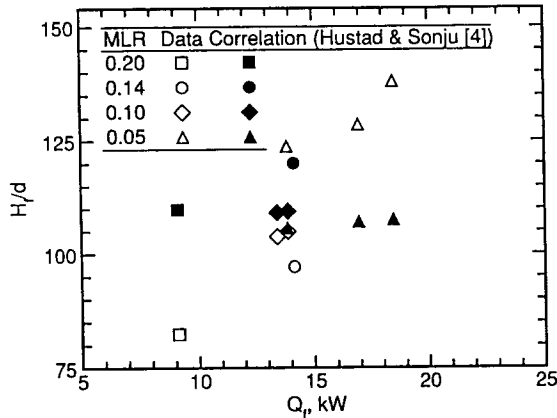


Fig. 5. Visible flame heights as a function of heat release rate for several methane-to-liquid ratios.

tive air entrainment rates with the decreasing influence of buoyancy. Depending upon which one of the two characteristic diameters is appropriate, the present flames would be in the buoyant or the forced jet regimes. Measurements of velocities at the exit would clarify this question. However, whether larger evaporation length affects flame lengths can be assessed by fixing the heat release rate and varying the liquid loading.

Figure 5 shows that for a fixed heat release rate of 14 kW, the flame height normalized by the external orifice diameter (4.76 mm) decreases with increasing MLR. This is in agreement with the smaller drops created by the enhanced atomization with increasing MLR leading to a shorter evaporation length. It also suggests that the changes in flame height with heat release rates are partly due to the two-phase flow effects unique to spray flames.

Flame heights obtained from the correlation of Hustad and Sonju [4] for methane gaseous jet flames are also plotted in Fig. 5. For large methane flames, the correlation for the flame height is given by

$$H_f/d = 21 Fr^{0.2},$$

where Fr is the Froude number calculated from the two-phase velocity based on the external orifice diameter (4.76 mm). As can be seen from Fig. 5, a systematic variation of 20%–40% exists for the different conditions. The Froude number has not been modified by the two-phase flow correction suggested by

Hustad and Sonju [4]. If used, it would show even higher differences between measured values and the correlation. However, the velocity and the diameter used are based on the two-phase density and the total mass flow rate exiting the external orifice. In the work of Hustad and Sonju [4], the gas exit velocity was used to calculate the Froude number. For the present conditions, this would lead to very low flame heights. The constant 21 in the correlation may be adjusted due to differences in the fuel. However, the qualitative discrepancies in flame height variation would persist. The correlations of Becker and Liang [17] based on gas flames were also tried, but overpredicted the flame heights by up to a factor of 2. Based on these observations, it is apparent that two-phase effects need to be considered in flame-height correlations for high-liquid-loading spray flames.

The radiative heat flux to a semiinfinite cylinder surrounding the flames was measured using a wide angle radiometer. The distance of the radiometer from the flame axis during the axial traverse was selected to be equal to the flame height  $H_f$  based on the scaling rule devised by Sivathanu and Gore [11]. The radiative heat flux was normalized by the total radiant output of the flame divided by the surface area of an imaginary sphere with radius equal to the distance from the detector to the flame axis. The normalized heat flux plotted as a function of the normalized axial distance is shown in Fig. 6. The data for the eight flames collapse extremely well on the plot of Fig. 6 suggesting that the radiation scaling of

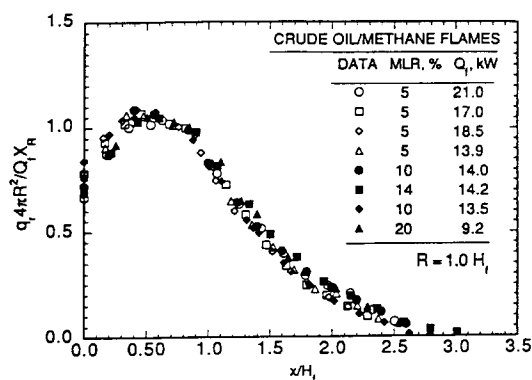


Fig. 6. Normalized radiative heat flux parallel to the axis of crude-oil/methane flames.

Sivathanu and Gore [11] is applicable to two-phase flames. The effects of different fuel properties (soot concentrations and temperature) are accounted for by the radiative fraction used in the scaling. The differences in geometry of the flame are accounted for by the use of the flame height. Therefore, the effects of two-phase flow are built into the scaling via the effects on flame height caused by different evaporation length requirements. As pointed out by Sivathanu and Gore [11] the collapse of Fig. 6 provides a convenient method for obtaining the total radiant output of a jet flame by making the radiation heat flux measurement at a single point.

As described in Table 1, the radiative fractions,  $X_R$ , vary between 10.2% and 21.4%. Figure 7a shows the  $X_R$  plotted as a function of the total heat release rate for a fixed MLR. The values of  $X_R$  are independent of the heat release rate for a fixed MLR. Figure 7b shows that  $X_R$  increases with decreasing MLR at a fixed heat release rate due to the propensity of crude oil flames to soot. The values of  $X_R$  are lower than expected. For buoyant methane jet

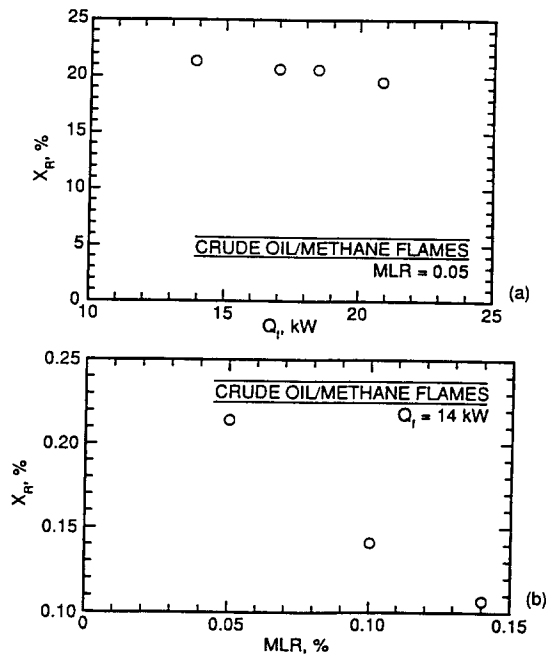


Fig. 7. Radiative heat loss fractions for crude-oil/methane flames as a function of heat release rate for a fixed methane-to-liquid ratio and as a function of methane-to-liquid ratio for a fixed heat release rate.

flames,  $X_R$  values of approximately 18% are reported in the literature (see Ref. 18 and references therein), for pool flames burning Alberta sweet crude oil a value of  $X_R = 30\%$  has been reported [5]. Thus the values of  $X_R$  for the present jet flames are unexpectedly low. Such low values can be realized if the flame temperatures are low due to incompleteness of combustion or if the sooting tendency of crude oil is substantially diminished in the present flame configuration. These questions can be discussed with the help of the emission and absorption data.

Figure 8 shows the measurements of emission temperature and transmittance for flames with MLRs of 14%, 10%, and 5%. These correspond to test cases 2, 4, and 5, respectively, in Table 1. The heat release rate is maintained at 14 kW for all cases. The uncertainties in the mean temperature measurements were about 10%, estimated by perturbing the signals from the flame by the RMS of the measurements during blackbody calibration. Since the measurements are path integrated, the temperature probe selects the peak temperature values

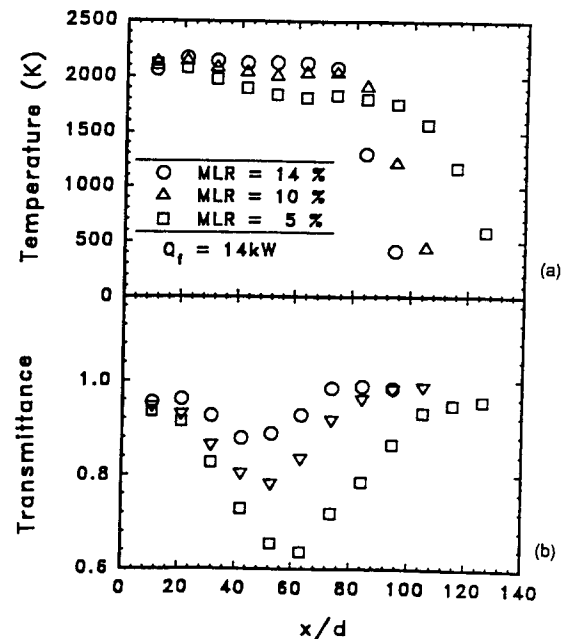


Fig. 8. Path-integrated emission temperature measurements and soot transmittance measurements for crude-oil/methane spray flames with methane-to-liquid ratio as a parameter.

along the path. For the highest methane loading the peak temperatures (see Fig. 8a) are approximately 2200 K near the injector exit and reduce to approximately 2150 K at approximately  $x/d = 70$  before decreasing beyond the flame tip. The small decrease in peak flame temperature is due to the relatively low radiative heat loss. The high peak temperatures represent almost complete combustion of the fuel. With increasing liquid loading, the peak temperatures decrease only slightly near the burner exit. For the lowest methane loading, the temperatures decrease by approximately 300 K with axial distance primarily due to radiative heat loss. The highest-liquid-loading flame shows emission due to soot until  $x/d = 120$ . The reduction in temperature decreases some of the expected increase in radiant output due to reduced transmittance with higher liquid loading.

The decrease in transmittance of the diametric path is shown in Fig. 8b. The transmittance for the highest-liquid-loading flame decreases to approximately 0.6 while those for the intermediate and low-liquid-loading cases are much higher. The overall decrease in transmittance causes the total radiant energy for the high-liquid-loading flame to increase from 10.2% to 21.4% (see Table 1) in spite of the reduction in temperature. The relatively high values of measured temperatures suggest that the reduced radiant loads are not due to incompleteness of combustion.

The basic reasons for reduced soot formation in the present spray configuration that contribute to reduced radiant heat loss are presently unknown. However, the basic understanding of soot formation and emission processes even in gaseous flames is such that the present work must be limited to reporting the first experimental observations for high liquid loading spray flames.

## CONCLUSIONS

The following conclusions can be drawn from the present study:

1. The effervescent atomizer-burner leads to efficient combustion in crude oil/methane/hydrogen flames with very high liquid loading.
2. The measurements of flame height showed systematic effects of liquid loading and atomization quality. The flame heights increase with increasing heat release rates and decreasing methane-to-liquid mass flow rate possibly due to the longer distance needed for evaporation of the drops.
3. The measurements of radiative fractions are unexpectedly low. Based on the emission temperature measurements, incompleteness of combustion does not play a role in the reduced radiative fractions. These data and relatively high measured transmittances suggest that reduced soot loading contributes to lower  $X_R$ .
4. Single-point radiation measurements following the scaling rule of Sivathanu and Gore [11] can be used to estimate the total radiant output for the two-phase flames.
5. Study of additional operating conditions, particularly those with increased residence time, are needed to obtain generalized global properties for crude oil/methane flames.

This study was partially supported by the National Institute of Standards and Technology, Building and Fire Research Laboratory under Grant No. 60NANB1D1172, with Dr. D. D. Evans serving as NIST Scientific Officer. The work regarding oil well fires at NIST is supported by the Mineral Management Service of the US Department of Interior with Mr. Charles Smith and Mr. Ed Tennyson serving as Program Managers.

## REFERENCES

1. Evans, D. D., and Pfenning, D., *Oil Gas J.* 83(no. 17):80-86 (1985).
2. Gore, J. P., and Evans, D. D., *OCS Study MMS 91-0057* (J. B. Gregory, C. E. Smith, and E. J. Tennyson, Eds.), United States Department of Interior, Washington, D.C., 1991.
3. Faeth, G. M., *Prog. Ener. Combust. Sci.* 13:293-345 (1987).
4. Hustad, H., and Sonju, O. K., *Prog. Astronaut. Aeronaut.* 105:365 (1986).
5. Gore, J. P., Klassen, M., Hamins, A., and Kashiwagi, T., *Fire Safety Science Proceedings of The Third International Symposium* (G. Cox and B. Langford, Eds.), Elsevier, London, 1991, p. 395.
6. Lund, M. T., Sojka, P. E., Lefebvre, A. H., and Gosselin, P. G., *Atom. Sprays* 3:77-89 (1993).
7. McCaffrey B. J., and Evans, D. D., *Twenty-First Symposium (International) on Combustion*, The Combustion Institute, Pittsburgh, 1986, p. 25.

8. Gore, J. P., Ph.D. thesis, The Pennsylvania State University, University Park, PA, 1986.
9. Masri, A. R., and Bilger, R. W., *Twenty-First Symposium (International) on Combustion*, The Combustion Institute, Pittsburgh, 1986, p. 1511.
10. Lund, M. T., Jian, C. Q., Sojka, P. E., Gore, J. P., and Panchagnula, M., *J. Fluids Eng.*, 1993, in revision for *ASME J. Fluids Eng.* Also to be presented at the ASME Winter Annual Meeting 1993, New Orleans.
11. Sivathanu, Y. R., and Gore, J. P., *Combust. Flame* 94:265-270 (1993).
12. Lund, M. T., MSME thesis, Purdue University, West Lafayette, IN, 1992.
13. Sivathanu, Y. R., Gore, J. P., and Dolinar, J., *Combust. Sci. Technol.* 76:45-66 (1991).
14. Dalzell, W. H., and Sarofim, A. F., *J. Heat Transf.* 91:100-104 (1969).
15. Sivathanu, Y. R., Gore, J. P., Janssen, J. M., Senser, D. W., *J. Heat Transf.* 115:653-658 (1993).
16. Rosin, P., and Rammler, E., *J. Inst. Fuel* 7(no. 31):29-36 (1933).
17. Becker, H. A., and Liang, D., *Combust. Flame* 32:115-137 (1978).
18. Faeth, G. M., Gore, J. P., Chuech, S. G., and Jeng, S. M., *Annual Review of Numerical Fluid Mechanics and Heat Transfer* (C. L. Tien and T. C. Chawla, Eds.), Hemisphere, New York, 1989, p. 1.

Received 27 May 1993; revised 9 December 1993